

Nickel(II) Nanoparticles Immobilized on EDTA-Modified Fe₃O₄@SiO₂ Nanospheres as Efficient and Recyclable Catalysts for Ligand-Free Suzuki–Miyaura Coupling of Aryl Carbamates and Sulfamates

Iman Dindarloo Inaloo,* Sahar Majnooni, Hassan Eslahi, and Mohsen Esmaeilpour



Cite This: *ACS Omega* 2020, 5, 7406–7417



Read Online

ACCESS |



Metrics & More

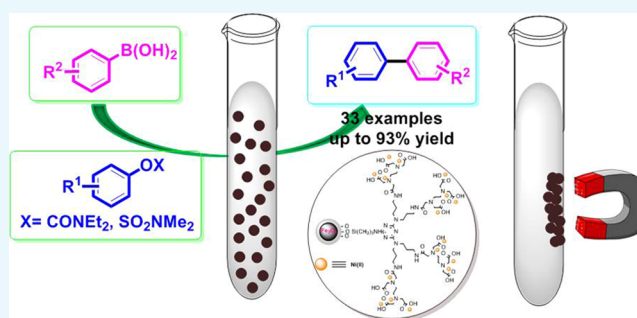


Article Recommendations



Supporting Information

ABSTRACT: A highly efficient and air-, thermal-, and moisture-stable nickel-based catalyst with excellent magnetic properties supported on silica-coated magnetic Fe₃O₄ nanoparticles was successfully synthesized. It was well characterized by Fourier transform infrared spectroscopy, powder X-ray diffraction, transmission electron microscopy, field emission scanning electron microscopy, thermogravimetric analysis, dynamic light scattering (DLS), X-ray photoelectron spectroscopy, vibration sample magnetometry, energy-dispersive X-ray analysis, inductively coupled plasma analysis, and nitrogen adsorption–desorption isotherm analysis. The Suzuki–Miyaura coupling reaction between aryl carbamates and/or sulfamates with arylboronic acids was selected to demonstrate the catalytic activity and efficiency of the as-prepared magnetic nanocatalyst. Using the mentioned heterogeneous nanocatalyst in such reactions generated corresponding products in good to excellent yields in which the catalyst could easily be recovered from the reaction mixture with an external magnetic field to reuse directly for the next several cycles without significant loss of its activity.



INTRODUCTION

“Nanotechnology is the sixth truly revolutionary technology introduced in the modern world”, D. Allan Bromley (1926–2005).¹ Nanotechnology has potentially changed our life and insights about it. Having many susceptibilities compared with other approaches, using nanotechnology is one of the main characteristics of modern scientific notions for the synthesis of novel structures.^{1,2} Nanoparticles (NPs) are interesting primary particles for scientists because of increased activity, modified structure, and surface area to volume ratio.³ Moreover, NPs have many advanced applications in electronic and optical industries, textile industries, drug delivery, medicine, and cosmetics.^{2–4}

Magnetic NPs (MNPs) are the important groups of functional NPs that have been broadly pursued owing to their interesting magnetic properties and attractive potential.^{5,6} The study of such nontoxic and biocompatible particles opens new ways to figure out their great potential in technological or industrial applications including medical therapeutics and diagnostics, magnetic data storage, environmental remediation, hyperthermia-based therapy of cancer, magnetic resonance imaging (MRI), and catalysis.⁷ Although these particles especially Fe₃O₄ NPs have many advantages; unfortunately, they tend to aggregate quickly because of anisotropic dipolar attractions and their applications face a big challenge.⁷

Therefore, using stabilizers as the shell is vital to control their size increases.^{8,9}

Among various shells, silica is one of the most trustable coating layers for Fe₃O₄ NPs adding to its chemical and thermal stability, high persistence in wide ranges of pH values, biocompatibility, and modified surface.^{8–11} Moreover, it enables organic compounds to be covalently attached to a library of intended NPs for interesting applications as a heterogeneous catalyst.¹² As a result, magnetic core–shell structures offer a wide range of applications in optics, catalysis, biomedicine, materials, environmental science, and energy as the leading edge of modern research and hot topics.^{13,14} Besides, having excellent properties such as versatility, biocompatibility, controllability, stability, and being inexpensive, they have attracted outstanding interest.^{13–15} Furthermore, they can be easily recovered and reused from the reaction mixture several times by external magnetic fields resulting in a low cost and green situation for the reaction progress.^{8–16}

Received: December 26, 2019

Accepted: March 16, 2020

Published: March 27, 2020



The carbon–carbon bond-formations are the foremost challenges in the synthesis of a wide ranges of natural and artificial products for pharmaceutical and agrochemical applications.^{17,18} In recent decades, the transition-metal cross-coupling reactions have played a major role in the development of designing efficient reactions.^{19,20} In this regard, a number of highly reactive metal catalysts have been developed and introduced for cross-coupling reactions.²¹ Moreover, the correlation of these developments with the principles of green chemistry concepts is very necessary and important.^{22,23} Concerns over contamination of residual toxic transition metals such as palladium in products and the high price of this catalyst led scientists to proliferate the use of economical and safer metal catalysts for such cross-coupling reactions.^{24,25} Since the late twentieth century when the nickel-catalyzed cross-coupling reaction of aryl halides and arylboronic acids was reported by Miyaura and co-workers for the first time, this reaction has attracted a lot of attention in academic and industrial research and has become one of the most powerful synthetic tools for the C–C bond formations.²⁶ Therefore, many efforts have recently been made to improve the efficiency and performance of this protocol.^{27–42} One of the most important achievements of these investigations is using phenol derivatives (aryl mesylates, tosylates, triflates, phosphates, sulfamates, carbonates, or carbamates) as the proper and effective alternatives to aryl halides in the C–C bond formation reactions.^{29–35} This achievement is so important because: (a) the aryl halides are generally not environmentally friendly and using such precursors produces halides as byproducts leading to environmental pollution, (b) the preparation of aryl halides often involves tedious steps, wasteful production processes, and harsh reaction conditions, and (c) the phenol derivatives are safer substrates, more accessible, and usually can be prepared on an industrial scale.^{29–40} However, this reaction still suffers from several limitations and drawbacks such as the necessity to employ additional quantities of ligands such as phosphine and carbenes, the high sensitivity of these ligands toward air and moisture, having expensive and multistep procedures for the synthesis of ligands, and high catalyst loading.^{41,42}

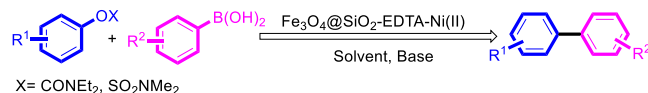
Conventionally, because of the high sensitivity of the Ni(0) complexes against air and moisture that is the main catalytic limitation in such reactions,^{43,44} these catalysts generally are being generated from Ni(II) complexes in the presence of reducing agents via *in situ* reactions.^{45,46} It should be noted that the use of reducing toxic agents is another disadvantage of these methods.⁴⁷ Fortunately, some effective methods without the necessity to apply any toxic reducing agent have been reported in recent years.^{48–52}

Therefore, based on the aforementioned considerations and also the continuation of our efforts for preparing effective magnetic catalytic systems,^{53–56} herein, we have reported the synthesis, characterizations, and employment of nickel(II) NPs immobilized on EDTA-modified Fe₃O₄@SiO₂ nanospheres (Fe₃O₄@SiO₂-EDTA-Ni(II)) as a reusable and efficient catalyst for the Suzuki–Miyaura coupling of various aryl carbamates and/or sulfamates with arylboronic acids under mild conditions (Scheme 1).

RESULTS AND DISCUSSION

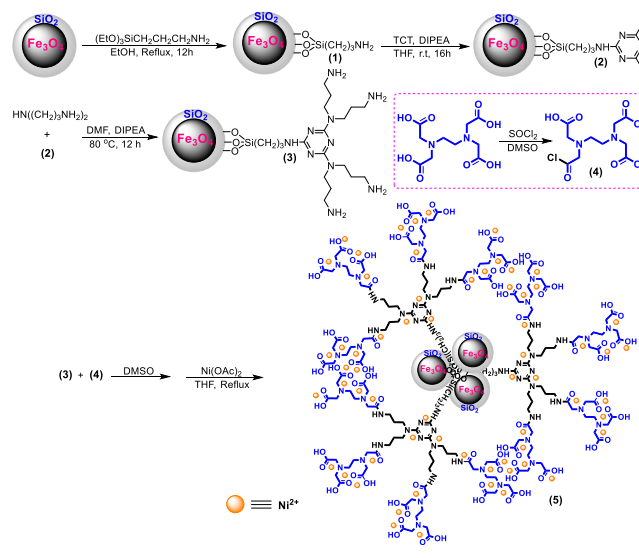
The nickel(II) particles were immobilized on EDTA-modified Fe₃O₄@SiO₂ nanospheres (Fe₃O₄@SiO₂-EDTA-Ni(II)) via

Scheme 1. Fe₃O₄@SiO₂-EDTA-Ni(II) as an Efficient and Recyclable Catalyst for the Suzuki Miyaura Cross-Coupling Reaction



the multistep procedure according to the procedure described in Scheme 2.

Scheme 2. Preparation of the Fe₃O₄@SiO₂-EDTA-Ni(II) Nanocatalyst



Subsequently, the prepared catalyst was well-characterized by the following instrumental techniques: Fourier transform infrared (FT-IR), powder X-ray diffraction (XRD), transmission electron microscopy (TEM), field emission scanning electron microscopy (FE-SEM), dynamic light scattering (DLS), energy dispersive X-ray (EDX), X-ray photoelectron spectroscopy (XPS), thermogravimetric analysis (TGA), vibrating sample magnetometer (VSM), Brunauer–Emmett–Teller (BET), inductively coupled plasma (ICP), and elemental analysis

The successful functionalization of the MNP surface was confirmed by examination of the FT-IR spectra. Figure 1 shows the FT-IR spectra of the Fe₃O₄@SiO₂, Fe₃O₄@SiO₂-NH₂, Fe₃O₄@SiO₂-TCT, Fe₃O₄@SiO₂-TCT-NH₂, Fe₃O₄@SiO₂-EDTA, and Fe₃O₄@SiO₂-EDTA-Ni(II) MNPs. These materials showed broad bands around 3400 and 580 cm⁻¹, which are the characteristic of O–H and Fe–O stretching bands, respectively.^{56,57} In the case of Fe₃O₄@SiO₂ NPs, the sharp band at 1090 cm⁻¹ is corresponded to Si–O–Si asymmetric stretching vibrations indicating the existence of silica in Fe₃O₄@SiO₂ NPs (Figure 1a).⁵⁸ The characteristic absorption bands at 2810–2986, 1489, 1123, and 576 cm⁻¹ attributed to C–H (stretching vibration), CH₂ (bending), Si–O–Si (stretching vibration), and Fe–O (stretching vibration) prove the existence of 3-aminopropyl(triethoxy)silane functional groups on the surface of the Fe₃O₄@SiO₂ NPs. Furthermore, the weak peaks at about 3300–3400 cm⁻¹ can be ascribed to NH₂ stretching vibrations (Figure 1b). In the spectrum of Fe₃O₄@SiO₂-TCT NPs, the characteristic adsorption at 1711, 1564, and 1511 cm⁻¹ are attributed to

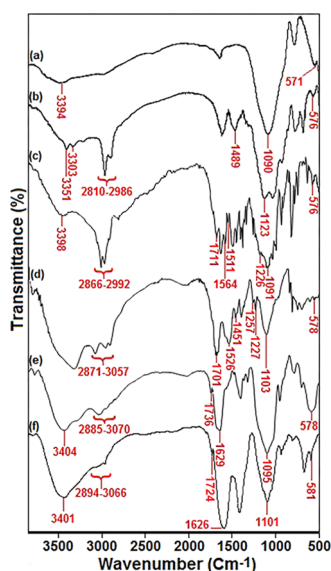


Figure 1. FT-IR spectra of (a) $\text{Fe}_3\text{O}_4@/\text{SiO}_2$, (b) $\text{Fe}_3\text{O}_4@/\text{SiO}_2\text{-NH}_2$, (c) $\text{Fe}_3\text{O}_4@/\text{SiO}_2\text{-TCT}$, (d) $\text{Fe}_3\text{O}_4@/\text{SiO}_2\text{-TCT-NH}_2$, (e) $\text{Fe}_3\text{O}_4@/\text{SiO}_2\text{-EDTA}$, and (f) $\text{Fe}_3\text{O}_4@/\text{SiO}_2\text{-EDTA-Ni(II)}$ NPs.

C=N stretching vibrations (Figure 1c). The peak at 1091 cm^{-1} was related to the C-Cl groups of cyanuric chloride, which is overlapped by the stretching vibrations of Si-O=Si groups in silica shells (Figure 1c). The FT-IR spectra of $\text{Fe}_3\text{O}_4@/\text{SiO}_2\text{-TCT-NH}_2$ NPs were characterized by the following absorption bands: stretching vibrations of C-N arising at 1257 cm^{-1} , CH_2 (bending) at 1451 cm^{-1} , and the C-H (symmetric and asymmetric stretching vibrations) at $2871\text{--}3057\text{ cm}^{-1}$ (Figure 1d). As can be seen, the typical absorption peak at 3397 cm^{-1} indicates the overlapped stretching vibrations of N-H and O-H bonds (Figure 1d). According to Figure 1e, the successful $\text{Fe}_3\text{O}_4@/\text{SiO}_2\text{-TCT-NH}_2$ surface modification with EDTA moieties was also verified. In the FT-IR spectra of $\text{Fe}_3\text{O}_4@/\text{SiO}_2\text{-EDTA}$ (Figure 1e), basic characteristic vibrations were observed for C-H bands (asymmetric and symmetric stretching) at $2885\text{--}3070\text{ cm}^{-1}$, Si-O-Si asymmetric stretching and symmetric stretching at 1095 and 801 cm^{-1} , respectively, and Fe-O (stretching vibration) at 578 cm^{-1} . Furthermore, the characteristic bands of carbonyl groups were observed at 1736 cm^{-1} (C=O carboxylic acid stretching vibration) and 1629 cm^{-1} (C=O amide stretching vibration). Eventually, in terms of $\text{Fe}_3\text{O}_4@/\text{SiO}_2\text{-EDTA-Ni(II)}$ (Figure 1f), a redshift of the band at 1736 cm^{-1} is observed ($1736\text{ cm}^{-1} \rightarrow 1724\text{ cm}^{-1}$), which is probably the characteristic of the carbonyl group after interaction with the nickel ions. Thus, the above results indicate that the functional groups were successfully grafted onto the surface of the magnetic $\text{Fe}_3\text{O}_4@/\text{SiO}_2$ NPs.

The crystalline structure of MNPs was identified with the XRD technique. As illustrated in Figure 2a, the XRD pattern exhibited reflection peaks at around $2\theta = 30.1, 35.4, 43.1, 53.4, 57.0,$ and 62.6° that can be indexed to (220), (311), (400), (422), (511), and (440) crystallographic planes of cubic Fe_3O_4 (JCPDS 88-0866).³⁰ However, the peak positions of the composite sample remain unchanged, revealing that the crystal phase of magnetic cores is well-maintained after the coating process. However, the crystallinity of the samples decreases after the coating process and the catalyst went toward an amorphous structure (Figure 2b,c). These results provide

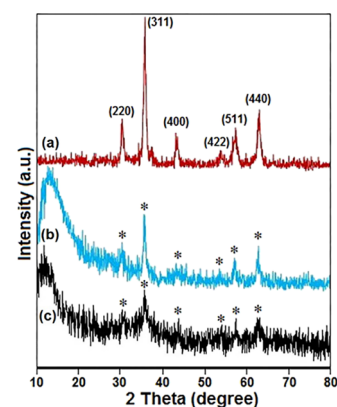


Figure 2. XRD diffraction pattern of (a) Fe_3O_4 , (b) $\text{Fe}_3\text{O}_4@/\text{SiO}_2$, and (c) $\text{Fe}_3\text{O}_4@/\text{SiO}_2\text{-EDTA-Ni(II)}$ NPs.

further evidence for the successful functionalization of the nanomagnetic surfaces. Furthermore, the XRD pattern of $\text{Fe}_3\text{O}_4@/\text{SiO}_2$ shows an obvious diffusion peak between 10 and 20° that appears because of the presence of amorphous silica (Figure 2b). For $\text{Fe}_3\text{O}_4@/\text{SiO}_2\text{-EDTA-Ni(II)}$ MNPs, the broad peak was transferred to lower angles due to the synergetic effect of amorphous silica and the dendrimer polymer (Figure 2c).

The morphologies, particle size, and structural features of the magnetic nanomaterials and the synthesized catalyst can be observed directly from the TEM and FE-SEM images (Figure 3a-c). The obtained magnetite particles possess a uniformly spherical shape and a mean diameter of $\sim 20\text{ nm}$ (Figure 3a,d). Coating silica over the Fe_3O_4 NPs was achieved via the well-known Stöber method. The TEM image of $\text{Fe}_3\text{O}_4@/\text{SiO}_2$ clearly shows the well-defined core-shell structure with a shell thickness of $\sim 10\text{ nm}$ (Figure 3b). Furthermore, the TEM image presented in Figure 3c indicates the structure of $\text{Fe}_3\text{O}_4@/\text{SiO}_2\text{-EDTA-Ni(II)}$ NPs. After being coated with the organic layer, the particle size of $\text{Fe}_3\text{O}_4@/\text{SiO}_2\text{-EDTA-Ni(II)}$ NPs was found to be 20 nm in diameter.

The FE-SEM photographs demonstrate that the $\text{Fe}_3\text{O}_4@/\text{SiO}_2$ and $\text{Fe}_3\text{O}_4@/\text{SiO}_2\text{-EDTA-Ni(II)}$ MNPs are in an almost regular spherical shape (Figure 3e,f). Moreover, these results are consistent with the particle-size distribution histogram of MNPs, which were in a narrow distribution in the range of $8\text{--}16, 16\text{--}24,$ and $23\text{--}37\text{ nm}$ and average size distribution of $12, 20,$ and 31 nm for $\text{Fe}_3\text{O}_4, \text{Fe}_3\text{O}_4@/\text{SiO}_2,$ and $\text{Fe}_3\text{O}_4@/\text{SiO}_2\text{-EDTA-Ni(II)}$ NPs, respectively (Figure 3g-i).

The existence of nickel in the $\text{Fe}_3\text{O}_4@/\text{SiO}_2\text{-EDTA-Ni(II)}$ catalyst was also confirmed by the EDX detector coupled to the SEM in which the presence of Fe, Si, C, N, and O can be confirmed clearly (Figure 4). The higher intensity of the Si peak compared with the Fe peaks indicates that the magnetite NPs were trapped by silica. According to the above analysis, it can be inferred that the $\text{Fe}_3\text{O}_4@/\text{SiO}_2\text{-EDTA-Ni(II)}$ has been successfully synthesized.

The TGA of the magnetic nanocatalyst was performed over the temperature range of $25\text{--}700^\circ\text{C}$. As shown in Figure 5A, the first weight loss for all samples, which occurred below 150°C , was attributed to the loss of adsorbed water molecules on the surface of nanostructured materials, and the second step occurred between about 150°C and nearly 600°C that is attributed to the decomposition of coating organic layers in the nanocomposite. As shown in Figure 5A(d), a significant weight loss of nearly 42.7% in the range of $150\text{--}600^\circ\text{C}$ was observed

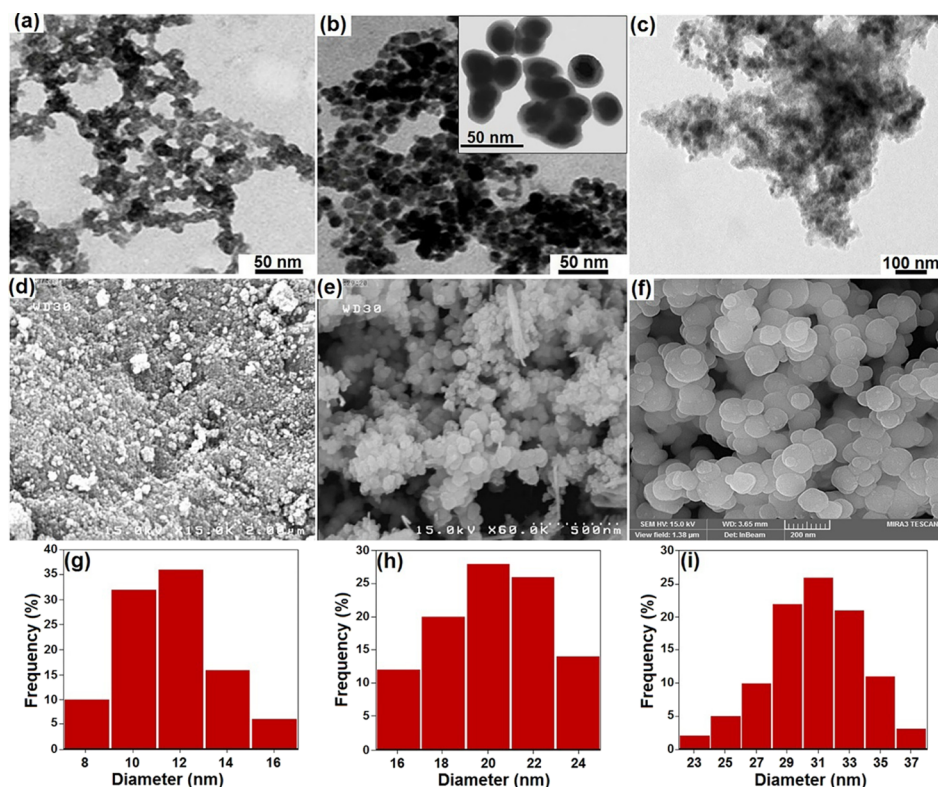


Figure 3. TEM images of (a) Fe_3O_4 , (b) $\text{Fe}_3\text{O}_4@SiO_2$, and (c) $\text{Fe}_3\text{O}_4@SiO_2-EDTA-Ni(II)$; FE-SEM images of (d) Fe_3O_4 , (e) $\text{Fe}_3\text{O}_4@SiO_2$, and (f) $\text{Fe}_3\text{O}_4@SiO_2-EDTA-Ni(II)$; and size distributions of (g) Fe_3O_4 , (h) $\text{Fe}_3\text{O}_4@SiO_2$, and (i) $\text{Fe}_3\text{O}_4@SiO_2-EDTA-Ni(II)$ NPs.

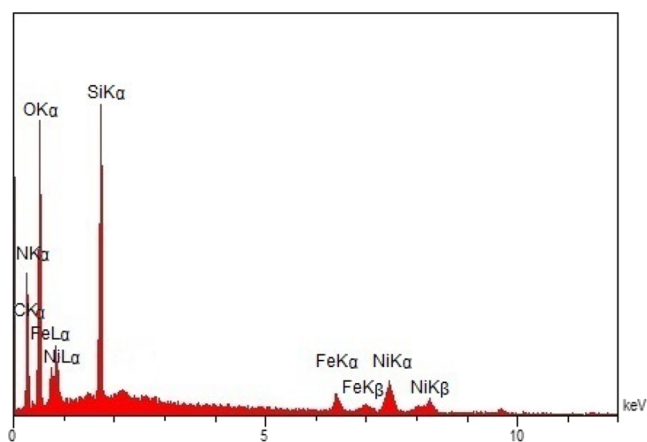


Figure 4. EDX spectrum of the $\text{Fe}_3\text{O}_4@SiO_2-EDTA-Ni(II)$ NPs.

for the sample catalyst due to the elimination of organic material over $\text{Fe}_3\text{O}_4@SiO_2$ NPs.

To study the magnetic properties of MNPs, the hysteresis loops of magnetite and functionalized magnetite NPs at room temperature were investigated by using a VSM. As shown in Figure 5B, no hysteresis was observed in the hysteresis loops of three materials, and the remanence and coercivity were nearly zero, exhibiting typical superparamagnetic behavior. The magnetizations of Fe_3O_4 and $\text{Fe}_3\text{O}_4@SiO_2-EDTA-Ni(II)$ MNPs were 64.8 and 28.7 emu/g, respectively (Figure 5B). The silica shell and other organic compounds cause a reduction in the magnetic strength of the composite owing to the weight contribution from the nonmagnetic portion. Nevertheless, $\text{Fe}_3\text{O}_4@SiO_2-EDTA-Ni(II)$ possesses excellent magnetic responsibility and suitable magnetization values, which can quickly respond to the external magnetic field and quickly disperse again when the external magnetic field is

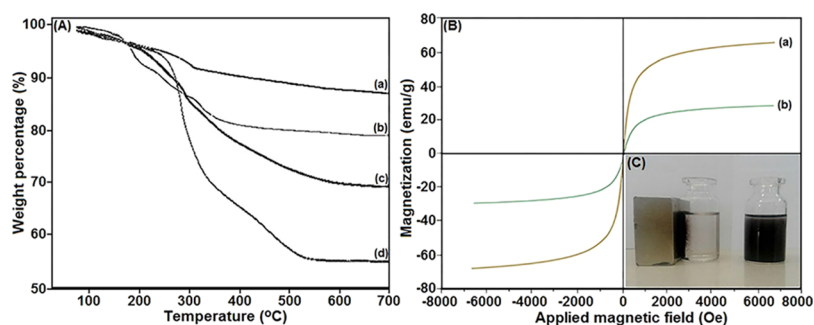


Figure 5. (A) TGA spectrum of (a) $\text{Fe}_3\text{O}_4@SiO_2-NH_2$, (b) $\text{Fe}_3\text{O}_4@SiO_2-TCT$, (c) $\text{Fe}_3\text{O}_4@SiO_2-TCT-NH_2$, and (d) $\text{Fe}_3\text{O}_4@SiO_2-EDTA-Ni(II)$ NPs; (B) magnetic hysteresis loops of (a) Fe_3O_4 and (b) $\text{Fe}_3\text{O}_4@SiO_2-EDTA-Ni(II)$ NPs; (C) good dispersity and easy separation of the catalyst by an external magnetic field.

removed (Figure 5C). These results exhibit the good magnetic properties of the nanocomposite, which is an advantage in our catalytic system for separation.

N₂ adsorption–desorption isotherms were obtained to investigate the porous structure and surface area of the NPs. The measured specific surface areas were 480, 430.3, and 392.6 m²/g for Fe₃O₄, Fe₃O₄@SiO₂, and Fe₃O₄@SiO₂–EDTA–Ni(II), respectively (Table 1). Also, the particle sizes of

Table 1. Selected Properties of Fe₃O₄, Fe₃O₄@SiO₂, and Fe₃O₄@SiO₂–EDTA–Ni(II) NPs

sample	Fe ₃ O ₄ crystal structure	specific surface area (m ² /g) ^a	magnetite particle size (nm) ^b
Fe ₃ O ₄	cubic spinel	480	11.33
Fe ₃ O ₄ @SiO ₂	cubic spinel	430.3	12.64
Fe ₃ O ₄ @SiO ₂ –EDTA–Ni(II)	cubic spinel	371.6	14.97

^aCalculated by the BJH method. ^bCalculated by the Scherrer equation based on XRD patterns.

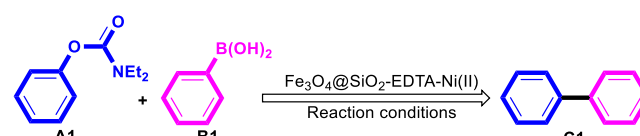
magnetite calculated using the Scherrer equation were 11.33, 12.64, and 14.97 nm for Fe₃O₄, Fe₃O₄@SiO₂, and Fe₃O₄@SiO₂–EDTA–Ni(II), respectively (Table 1).

Elemental analyses for Fe₃O₄@SiO₂–NH₂, Fe₃O₄@SiO₂–TCT, Fe₃O₄@SiO₂–TCT–NH₂, and Fe₃O₄@SiO₂–EDTA–Ni(II) were carried out, and the data are tabulated in Table 2 which are in good agreement with the result obtained from TGA. These obtained results displayed that the contents of C, H, and N for Fe₃O₄@SiO₂–EDTA–Ni(II) are 21.61, 2.87, and 9.232%, respectively.

Additionally, Ni loading of the catalyst was confirmed by the ICP analyzer. For this purpose, the catalyst (1 g) was stirred in aq. HCl (37%), then the magnetic nanocomposite was separated by an external magnetic field and the remaining solution was analyzed by ICP to determine the content of nickel. The amount of Ni on the support was determined as (0.55) mmol per gram of the catalyst.

After the preparation and detailed characterization of Fe₃O₄@SiO₂–EDTA–Ni(II), the efficiency of the synthesized nanocatalyst on cross-coupling reactions to form C–C bonds was evaluated. To find the effective reaction conditions, the model reaction between phenyl carbamate (A1) with phenylboronic acid (B1) using the proposed catalytic system was investigated (Table 3). Various factors such as solvents, bases, catalyst loadings, temperature, and reaction time were tested, and the results have been depicted in Table 3. The solvent

Table 3. Optimization Studies for Cross-Coupling of Phenyl Carbamate with Phenylboronic Acid^a



entry	base (equiv)	solvent	temp (°C)	yield (%) ^b
1	NaOC ₂ H ₄ OH(2.0)	H ₂ O	reflux	43
2	NaOC ₂ H ₄ OH(2.0)	ethanol	reflux	56
3	NaOC ₂ H ₄ OH(2.0)	n-PrOH	reflux	52
4	NaOC ₂ H ₄ OH(2.0)	EG	100	91
5	NaOC ₂ H ₄ OH(2.0)	glycerol	100	73
6	NaOC ₂ H ₄ OH(2.0)	dioxane	reflux	37
7	K ₃ PO ₄ (2.0)	EG	100	83
8	NaOH (2.0)	EG	100	72
9	K ₂ CO ₃ (2.0)	EG	100	80
10	Cs ₂ CO ₃ (2.0)	EG	100	79
11	DBU (2.0)	EG	100	69
12	DABCO (2.0)	EG	100	66
13	NaO ^t Bu (2.0)	EG	100	89
14	NaOC ₂ H ₅ (2.0)	EG	100	84
15		EG	100	0
16	NaOC ₂ H ₄ OH(1.0)	EG	100	70
17	NaOC ₂ H ₄ OH(1.5)	EG	100	79
18	NaOC ₂ H ₄ OH(2.5)	EG	100	90
19	NaOC ₂ H ₄ OH(3.0)	EG	100	91

^aReaction conditions: phenyl carbamate (1 mmol), phenylboronic acid (1 mmol), base, Fe₃O₄@SiO₂–EDTA–Ni(II) catalyst(0.018 g, 1 mol %), solvent, 6 h ^bIsolated yield.

evaluation for the model reaction showed that using ethylene glycol (EG) as the solvent presents the highest yield (Table 3, entry 4). Moreover, the desired product, C1 was not observed when no base was added (Table 3, entry 15). This experiment showed that the presence of a base is crucial to have an efficient reaction. Therefore, we decided to investigate the series of organic and inorganic bases that are commonly used in the coupling reactions (Table 3, entries 4, 7–14). Based on these experiments, the best efficiency and performance were observed in the presence of EG monosodium salt (NaOC₂H₄OH) as the base (Table 3, entry 4). Also, it seems that the reaction efficiency depends on the amount of NaOC₂H₄OH and the highest yields were observed when its amount was 2 mmol (Table 3, entry 4). It should be noted that higher amount of the base did not present better yields of the desired product (Table 3, entries 18, 19). To improve the yield of the cross-coupling reaction, we also checked the catalyst

Table 2. TGA and Elemental Analysis for Fe₃O₄@SiO₂–NH₂, Fe₃O₄@SiO₂–TCT, Fe₃O₄@SiO₂–TCT–NH₂, and Fe₃O₄@SiO₂–EDTA–Ni(II) NPs

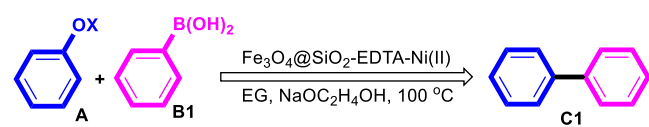
sample		C (%)	H (%)	N (%)	total (%) ^a
Fe ₃ O ₄ @SiO ₂ –NH ₂	TGA (wt %)	6.746	1.501	2.627	10.874
	EA (wt %)	6.614	1.475	2.532	10.621
Fe ₃ O ₄ @SiO ₂ –TCT	TGA (wt %)	7.377	0.717	5.736	3.830
	EA (wt %)	7.468	0.750	5.627	13.845
Fe ₃ O ₄ @SiO ₂ –TCT–NH ₂	TGA (wt %)	16.172	2.918	10.564	29.654
	EA (wt %)	15.946	2.871	10.377	29.194
Fe ₃ O ₄ @SiO ₂ –EDTA–Ni(II)	TGA (wt %)	22.821	2.853	9.112	34.786
	EA (wt %)	21.611	2.871	9.232	33.714

^aTotal (%) = C (%) + H (%) + N (%).

loading (Table S1), temperature (Table S3), and reaction time (Table S3) on the model reaction and the best results have been obtained using 0.02 g of $\text{Fe}_3\text{O}_4@\text{SiO}_2\text{-EDTA-Ni(II)}$ catalyst (1 mol % Ni(II)) at 100 °C after 6 h (Table 3, entry 4).

After getting the optimized conditions, we tested different phenol-based electrophiles in Ni-catalyzed Suzuki–Miyaura cross-coupling reactions to determine the high proficiency and generality of this catalytic system (Table 4). Although the

Table 4. Survey of Pseudo Halide Substrates^a



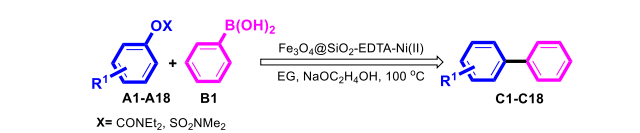
entry	X	yield (%) ^b
1	Me	0
2	Ac	43
3	Piv	47
4	Ms	54
5	Ts	62
6	Tf	57
7	CO ₂ ^t Bu	75
8	SO ₂ NEt ₂	89
9	CONEt ₂	91

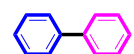
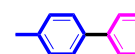
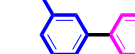
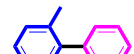
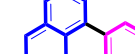
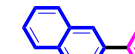
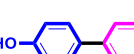
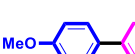
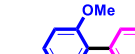
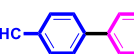
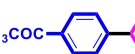
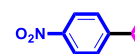
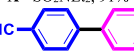
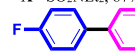
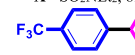
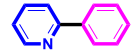
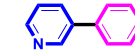
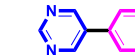
^aReaction conditions: phenol-based electrophiles (1 mmol), phenylboronic acid (1 mmol), NaOC₂H₄OH (2.0 mmol), $\text{Fe}_3\text{O}_4@\text{SiO}_2\text{-EDTA-Ni(II)}$ catalyst (0.018 g, 1 mol %), EG (3 mL), 100 °C, 6 h.
^bIsolated yield.

usage of aryl methyl ether did not lead to the production of the desired product under the optimized reaction conditions (Table 4, entry 1), moderate yields were observed when the phenol derivatives such as phenyl acetate, phenyl pivalate, phenyl mesylate, phenyl tosylate, and phenyl triflate were used as the electrophile (Table 4, entries 2–6). Accordingly, phenyl carbonate furnished the desired product in good yields (Table 4, entry 7). Finally, it was determined that the corresponding carbamate and sulfamate substrates introduced the coupling product in the highest yield (Table 4, entries 8 and 9). Thus, we elected the aryl carbamates and sulfamates as the suitable electrophiles for continuing the research.

The optimal reaction conditions were identified and then, we decided to investigate the scope, generality, and efficiency of this method for C–C bond formation. At first, we started from the treatment of a series of aryl carbamates and sulfamates in the reaction with phenylboronic acid (Table 5). Satisfyingly, both electron-donating and withdrawing groups on the phenyl ring of aryl carbamates and sulfamates efficiently produced the desired products in good to excellent yields (Table 5). It should be noted that a lower yield was observed in the case of ortho-substituted aryl carbamates and sulfamates in comparison to meta- and para-substituted ones, which might be due to steric factors (Table 5, entries C4 and C9). It is also noteworthy that the naphthyl carbamates and sulfamates display high reactivity leading to the corresponding cross-coupled biaryl products in high yields (Table 5, entries C5 and C6). Although pyridinyl and pyrimidinyl derivatives generally deactivate the transition-metal catalysts, especially in the nickel-based catalysts, our system was also suitable for these kinds of substrates and the desired coupling products

Table 5. Substrate Scope of Aryl Carbamates and Sulfamates^a



 C1 X = CONEt ₂ , 91% ^b X = SO ₂ NEt ₂ , 89% ^b	 C2 X = CONEt ₂ , 92% ^b X = SO ₂ NEt ₂ , 91% ^b	 C3 X = CONEt ₂ , 88% ^b X = SO ₂ NEt ₂ , 90% ^b
 C4 X = CONEt ₂ , 81% ^b X = SO ₂ NEt ₂ , 80% ^b	 C5 X = CONEt ₂ , 84% ^b X = SO ₂ NEt ₂ , 81% ^b	 C6 X = CONEt ₂ , 87% ^b X = SO ₂ NEt ₂ , 89% ^b
 C7 X = CONEt ₂ , 83% ^b X = SO ₂ NEt ₂ , 84% ^b	 C8 X = CONEt ₂ , 86% ^b X = SO ₂ NEt ₂ , 87% ^b	 C9 X = CONEt ₂ , 79% ^b X = SO ₂ NEt ₂ , 80% ^b
 C10 X = CONEt ₂ , 89% ^b X = SO ₂ NEt ₂ , 91% ^b	 C11 X = CONEt ₂ , 88% ^b X = SO ₂ NEt ₂ , 87% ^b	 C12 X = CONEt ₂ , 86% ^b X = SO ₂ NEt ₂ , 89% ^b
 C13 X = CONEt ₂ , 92% ^b X = SO ₂ NEt ₂ , 93% ^b	 C14 X = CONEt ₂ , 89% ^b X = SO ₂ NEt ₂ , 84% ^b	 C15 X = CONEt ₂ , 93% ^b X = SO ₂ NEt ₂ , 92% ^b
 C16 X = CONEt ₂ , 85% ^b X = SO ₂ NEt ₂ , 84% ^b	 C17 X = CONEt ₂ , 83% ^b X = SO ₂ NEt ₂ , 82% ^b	 C18 X = CONEt ₂ , 80% ^b X = SO ₂ NEt ₂ , 82% ^b

^aReaction conditions: aryl carbamates or sulfamates (1 mmol), phenylboronic acid (1 mmol), NaOC₂H₄OH (2.0 mmol), $\text{Fe}_3\text{O}_4@\text{SiO}_2\text{-EDTA-Ni(II)}$ catalyst (0.018 g, 1 mol %), EG (3 mL), 100 °C, 6 h. ^bIsolated yield.

were produced in significant yields (Table 5, entries C16–C18).

Inspired from interesting results achieved, we also decided to examine the effects of different substituents on the phenyl ring of aryl boronic acids under the optimal reaction conditions (Table 6). Arylboronic acids bearing various functional groups were compatible with this reaction system and the corresponding products were obtained in good to excellent yields (Table 6, entries C19–C33). However, the precursors with an electron-withdrawing group are somehow less effective than other arylboronic acids under these reaction conditions (Table 6, entries C26–C29). It is noteworthy that in the case of 2-methylphenylboronic acid, lower yield was obtained and it may be due to steric hindrance (Table 6, entry C22). Interestingly, we found that the heterocyclic boronic acids such as thiophen-2-ylboronic acid also worked efficiently under this catalytic system (Table 6, entries C30–C33).

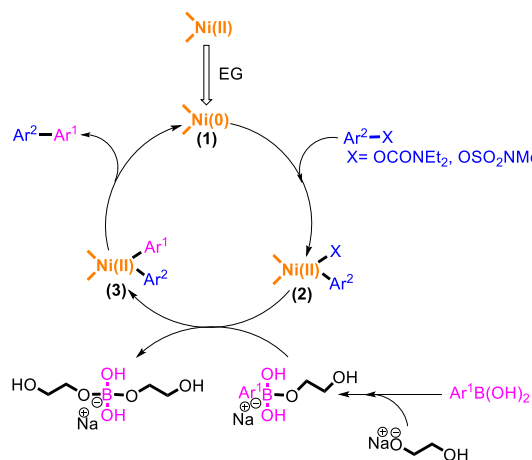
According to the reported research in the literature, we proposed a plausible catalytic mechanism for the Suzuki–Miyaura coupling of aryl carbamates or aryl sulfamates with arylboronic acids (Scheme 3).^{59–62} Initially, the process begins with the reduction of Ni(II) with EG as the reducing agent to provide the active Ni(0) species. Subsequently, the catalytic cycle starts with the oxidative addition of Ni(0) to aryl carbamates or aryl sulfamates to generate the intermediate, (1)

Table 6. Substrate Scope of Arylboronic Acids^a

C19 X = CONEt ₂ , 87% ^b X = SO ₂ NEt ₂ , 88% ^b	C20 X = CONEt ₂ , 90% ^b X = SO ₂ NEt ₂ , 92% ^b	C21 X = CONEt ₂ , 89% ^b X = SO ₂ NEt ₂ , 88% ^b
C22 X = CONEt ₂ , 81% ^b X = SO ₂ NEt ₂ , 80% ^b	C23 X = CONEt ₂ , 92% ^b X = SO ₂ NEt ₂ , 93% ^b	C24 X = CONEt ₂ , 84% ^b X = SO ₂ NEt ₂ , 86% ^b
C25 X = CONEt ₂ , 87% ^b X = SO ₂ NEt ₂ , 89% ^b	C26 X = CONEt ₂ , 83% ^b X = SO ₂ NEt ₂ , 82% ^b	C27 X = CONEt ₂ , 82% ^b X = SO ₂ NEt ₂ , 83% ^b
C28 X = CONEt ₂ , 84% ^b X = SO ₂ NEt ₂ , 85% ^b	C29 X = CONEt ₂ , 82% ^b X = SO ₂ NEt ₂ , 81% ^b	C30 X = CONEt ₂ , 81% ^b X = SO ₂ NEt ₂ , 83% ^b
C31 X = CONEt ₂ , 83% ^b X = SO ₂ NEt ₂ , 82% ^b	C32 X = CONEt ₂ , 84% ^b X = SO ₂ NEt ₂ , 83% ^b	C33 X = CONEt ₂ , 80% ^b X = SO ₂ NEt ₂ , 81% ^b

^aReaction conditions: aryl carbamates or sulfamates (1 mmol), aryl boronic acids (1 mmol), NaOC₂H₄OH (2.0 mmol), Fe₃O₄@SiO₂-EDTA-Ni(II) catalyst (0.018 g, 1 mol %), EG (3 mL), 100 °C, 6 h.
^bIsolated yield.

Scheme 3. Proposed Mechanism of Suzuki–Miyaura Cross-Coupling of Aryl Carbamates and Aryl Sulfamates



in situ. The transmetalation step occurs by the conversion of intermediate (1) to a nucleophilic intermediate, (2) in the presence of the base EG monosodium salt (NaOC₂H₄OH). This complex subsequently reacts with an organoboron compound which facilitates the aryl group transfer to reach the diaryl intermediate, (3). Finally, the formation of a C–C bond through the reductive elimination step generates the Ni(0) catalyst.

To determine the oxidation state of nickel, high-resolution XPS spectra of Ni 2p core levels were obtained from the catalyst before and after the reaction (Figure 6). According to the fitted data, the deconvoluted peaks at the binding energies

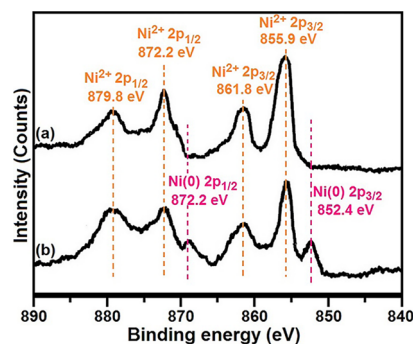


Figure 6. XPS spectra of the (a) fresh and (b) reused catalyst.

855.9 and 861.8 eV are attributed to Ni 2p_{3/2} and peaks at 872.2 and 879.8 eV are attributed to Ni 2p_{1/2} for the fresh catalyst that can be indexed to Ni²⁺ (Figure 6a).⁶³ Besides, the XPS patterns of the recovered catalyst show the peaks of both Ni²⁺ and Ni(0) (Figure 6b). The peaks at around 852.4 and 872.2 eV were assigned to the Ni 2p_{3/2} and Ni 2p_{1/2} levels in the Ni(0) which are in good agreement with the literature report.⁶⁴ The above phenomena supported that the reaction proceeded via the traditional Ni²⁺/Ni(0) cycle mechanism.

The recyclability and high stability of the economically and eco-friendly catalytic systems are very important in the industry and designing green and effective synthetic pathways. Therefore, we investigated these important factors in our catalyst. First, the reusability of the catalyst in the model reaction was studied and tested (Figure 7a). After completion

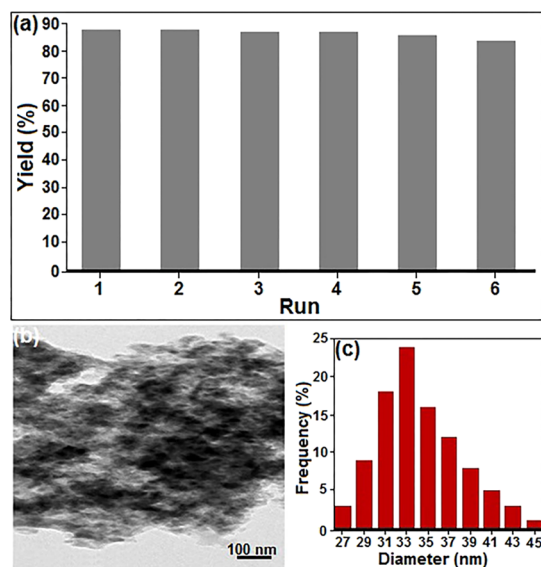


Figure 7. (a) Reusability of the catalyst for the Suzuki–Miyaura cross-coupling; (b) TEM and (c) DLS images of Fe₃O₄@SiO₂-EDTA-Ni(II) after the sixth recycling experiment.

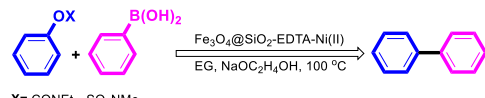
of the model reaction, the catalyst was easily separated by using an external magnetic field, washed twice with ethanol, and dried in an oven. Then, the recovered catalyst was used for the next runs with the same substrates. As shown in Figure 7a, the recovered Fe₃O₄@SiO₂-EDTA-Ni(II) exhibited almost constant catalytic activity for at least six runs in the model reaction and significant reduction in catalytic efficiency was not observed. Additionally, the TEM micrographs for the MNPs after the sixth cycle are displayed in Figure 7b. As revealed in

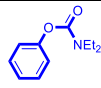
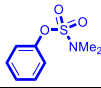
this figure, almost all $\text{Fe}_3\text{O}_4@\text{SiO}_2\text{-EDTA-Ni(II)}$ particles have the morphology and size the same as the fresh catalyst, indicating that the aggregation of NPs is venial. Eventually, the hydrodynamic diameter of the catalyst was investigated by the DLS technique (Figure 7c) in which this size distribution is centered at a value of 33 nm.

Additionally, the catalyst after the last run was investigated by ICP analysis to determine the amount of nickel leaching. Accordingly, the amount of loaded nickel on the recovered catalyst was measured to be 0.54 mmol/g. Propitiously, the ICP analysis after the seventh run showed less than 1% nickel leaching. Moreover, to determine the stability of the catalytic systems in the model reaction and the responsibility of nickel moiety for carrying out the model reaction, a hot filtration test was performed. When the reaction time of the model reaction reached the half time of reaction quenching, the catalyst NPs were taken out from the reaction mixture by an external magnetic field, the residue was allowed to stir under the reaction conditions. The monitoring of the reaction mixture by TLC did not show any considerable progress. These results showed that only a few species of nickel may exist in the solution phase and the main responsible species that catalyzes the model reaction is the $\text{Fe}_3\text{O}_4@\text{SiO}_2\text{-EDTA-Ni(II)}$ NPs. All of these data confirmed the high stability and reusability of the catalyst under these reaction conditions.

According to the wonderful results obtained, the application of the presented efficient strategy was also checked out for the preparation of biphenyl (C1) in different scales (1, 50, and 200 mmol). The obtained results are presented in Table 7 in which the capability of this method was proved to find efficient large-scale laboratory syntheses with the yield of trials at small scales.

Table 7. Comparison of Cross-Coupling of Phenyl Carbamate or Sulfamate with Phenylboronic Acid at Different Scales



substrate	Amount of substrate (mmol)	Time (h)	Yield (%) ^a
	1	6	89
	50	6	84
	200	8	83
	1	6	87
	50	6	83
	200	8	82

^aIsolated yield.

In the end, we decided to compare the capability of the proposed nanocatalyst in the synthesis of aryl carbamates and sulfamates with those reported in the literature (Table 8). As can be seen, almost all reports have applied toxic solvents with more reaction times and temperatures. In addition, they showed less reactivity against such reactions and also, fewer yields have been observed (Table 8, entries 1–4, 7–9). Although there are lower reaction times reported (Table 8, entries 5, 6), the observed yields are somehow less than the present work. Moreover, the reaction conditions for these are harsher. From the point of view of the recovery and reusability of the catalyst, this catalyst can be recovered and reused for

consequent reactions but other reports applied the catalyst with no recovery ability.

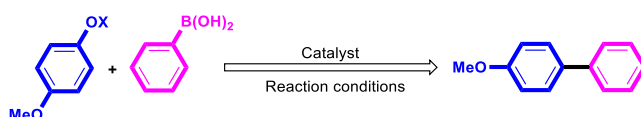
CONCLUSIONS

In summary, we have proposed a facile and effective method to prepare a magnetic nanocatalyst ($\text{Fe}_3\text{O}_4@\text{SiO}_2\text{-EDTA-Ni(II)}$) with characterization by various techniques. The catalyst demonstrated great performance in the Suzuki–Miyaura coupling reaction of aryl carbamates and/or sulfamates with arylboronic acids under mild reaction conditions. The methodology complements the more established methods without using external ligands or reducing agents. Also, a wide range of substrate scope was applied, even the presence of electron-rich substrate. Additionally, the catalyst can be easily recovered in a very short time using an external magnet and directly reused for six cycles with no significant loss in catalyst activity. Considering the improved economic and environmental benefits, this methodology was presented here to show its attractive features in using sulfamate and carbamate substrates as highly regarded precursors, especially in the pharmaceutical industry.

EXPERIMENTAL SECTION

Chemicals and Instrumentation. Chemical materials with high purity were purchased from Fluka and Merck. The reaction monitoring was accomplished by thin-layer chromatography (TLC) on gel F254 plates. Melting points were obtained with a micro melting point apparatus (electrothermal, BUCHI 510). NMR spectra were recorded in CDCl_3 on a Bruker Avance DPX 250 spectrometer using TMS as the internal standard. FT-IR spectra were collected on a Shimadzu FT-IR 8300 spectrometer using KBr pellets. XRD patterns were recorded in a Bruker AXS D8-advance powder X-ray diffractometer using $\text{Cu K}\alpha$ radiation. The TEM images were recorded using a Philips EM208 transmission electron microscope operated at 80 kV accelerating voltage. FE-SEM characterization was performed on a Hitachi S-4160 operated at a 20 kV accelerating voltage. DLSs were performed using a HORIBA-LB550. The surface composition was investigated using XPS on XR3E2 (VG Microtech) spectrometer using a Mg and Al twin anode X-ray gun with a multichannel detector and a hemispherical analyzer with a resolution of 1.0 eV. The BET surface area of the material was measured by the nitrogen adsorption isotherm method (BET; Micromeritics ASAP 2000). The magnetic properties of Fe_3O_4 MNPs and $\text{Fe}_3\text{O}_4@\text{SiO}_2\text{-EDTA-Ni}$ magnetic nanocomposites were analyzed using the MDK instrument model 7400 VSM. The TGA was performed on a NETZSCH STA 409 PC/PG instrument. The nickel amount on the carriers was measured by ICP–atomic emission spectrometry (ICP–AES). The elemental analyses (C, H, N) were obtained using a Flash EA-1112 CHNSO analyzer. Therefore, all products were identified by comparison of their spectral data and physical properties such as ^1H and ^{13}C NMR, CHNS, and melting points with those of the authentic sample and all yields refer to isolated products.

Synthesis of Silica-Coated MNPs ($\text{Fe}_3\text{O}_4@\text{SiO}_2\text{NPs}$). Magnetic (Fe_3O_4) NPs were synthesized according to our previous reports.^{54–56} In brief, $\text{FeCl}_3\cdot 6\text{H}_2\text{O}$ (1.3 g, 4.8 mmol), $\text{FeCl}_2\cdot 4\text{H}_2\text{O}$ (0.9 g, 4.5 mmol), and poly(vinyl alcohol) (PVA 15,000, 1 g) as the surfactant were dissolved in 30 mL of deionized water with vigorous mechanical stirring at 80 °C for

Table 8. Comparison with Reported Results for Suzuki–Miyaura Cross-Coupling Reactions between Phenylboronic Acid and 4-Methoxyphenyl Carbamates or Sulfamates

entry	X	catalyst	reaction conditions	time	yield (%)	reusability	refs
1	CONEt ₂	triazine-based Ni(II) PNP pincer complexes (2 mol %)	toluene/K ₃ PO ₄ /120–135 °C	16 h	84		65
2	CONEt ₂	NiCl ₂ (PCy ₃) ₂ (10 mol %)	toluene/K ₃ PO ₄ /110 °C	24 h	41		66
3	SO ₂ NMe ₂	NiCl ₂ (PCy ₃) ₂ (10 mol %)	toluene/K ₃ PO ₄ /110 °C	24 h	80		66
4	SO ₂ NMe ₂	dppf Ni(II) (<i>o</i> -tol) (Cl) (2.5 mol %)	toluene/K ₃ PO ₄ /80 °C	24 h	72		52
5	CONEt ₂	Ni(PCy ₃) ₂ Cl ₂ (5 mol %)	toluene/K ₃ PO ₄ /MW, 180 °C	10 min	67		67
6	SO ₂ NMe ₂	Ni(PCy ₃) ₂ Cl ₂ (5 mol %)	toluene/K ₃ PO ₄ /MW, 180 °C	10 min	70		67
7	SO ₂ NMe ₂	NiCl ₂ (dppp) (2 mol %)	dioxane/K ₃ PO ₄ /110 °C	24 h	35		68
8	SO ₂ NMe ₂	NiCl ₂ (dppf) (5 mol %)	toluene/K ₃ PO ₄ /110 °C	24 h	68		69
9	CONMe ₂	NiCl ₂ (dppf) (5 mol %)	toluene/K ₃ PO ₄ /110 °C	24 h	19		69
10	CONEt ₂	Fe ₃ O ₄ @SiO ₂ -EDTA-Ni(II) (1 mol %)	EG/NaOC ₂ H ₄ OH/100 °C	6	86	Yes	this work
11	SO ₂ NMe ₂	Fe ₃ O ₄ @SiO ₂ -EDTA-Ni(II) (1 mol %)	EG/NaOC ₂ H ₄ OH/100 °C	6	87	Yes	this work

30 min. Then, hexamethylenetetramine (1.0 mol) was slowly added to the solution and the solution pH was maintained at 10. The mixture was held at 80 °C in a water bath for 2 h with constant stirring and then, the black magnetite was collected by applying an external magnetic field and was rinsed with ethanol several times and dried under vacuum at 80 °C for 10 h. In the next step, for the synthesis of Fe₃O₄@SiO₂, 0.5 g of the synthesized Fe₃O₄ NPs were dispersed in a mixture containing ethanol (50 mL), deionized water (5 mL), and tetraethoxysilane (0.20 mL) in a glass reactor by using ultrasound irradiation.^{55–58} Then, NaOH (10 wt %, 5 mL) was added to the mixture and stirred at room temperature for 30 min. The resulting Fe₃O₄@SiO₂ NPs were collected by an external magnet, washed with distilled water and ethanol, and dried in a vacuum oven at 80 °C for 10 h.

Synthesis of Fe₃O₄@SiO₂-NH₂NPs.⁵⁸ To a suspension of SiO₂-coated magnetite particles (1 g) in ethanol (10 mL), 3-aminopropyl(triethoxy)silane (1 mmol, 0.25 mL) was added. The mixture was refluxed for 12 h, and then, it was cooled to room temperature to obtain a brown precipitate. The obtained solid was separated with an external magnet, washed with water and ethanol (1:1) to remove unreacted species, and dried under vacuum at 80 °C.

Synthesis of Fe₃O₄@SiO₂-TCT NPs. In a typical procedure, 1 g of the as-prepared Fe₃O₄@SiO₂-NH₂ NPs was first dispersed in 10 mL of THF containing 1 mmol (0.185 g) cyanuric chloride (TCT) and 1 mmol (0.17 mL) of diisopropylethylamine (DIPEA). Then, the obtained crude was stirred at room temperature for 16 h. Next, the modified NPs by cyanuric chloride were collected by magnetic field and washed 3 times with distilled water and ethanol solution. Finally, the resultant was dried at 60 °C for 4 h.

Synthesis of Fe₃O₄@SiO₂-TCT-NH₂ NPs. In a typical preparation procedure, bis(3-aminopropyl)amine (2 mmol, 0.25 mL) and DIPEA (2 mmol, 0.35 mL) were added to DMF (5 mL) containing cyanuric chloride-immobilized Fe₃O₄@SiO₂-NH₂NPs (1.0 g). After stirring at 80 °C for 12 h, the precipitate (Fe₃O₄@SiO₂-TCT-NH₂) was collected from the solution using a magnet, washed with water and ethanol several times, and dried at 70 °C for 4 h.

Synthesis of Fe₃O₄@SiO₂-EDTA-Ni(II) NPs. First, EDTA (2 mmol) was dispersed in DMSO (15 mL). Then, the solution of thionyl chloride (SOCl₂) (2 mmol) in DMSO

(5 mL) was added dropwise into the solution under vigorous stirring. Afterward, Fe₃O₄@SiO₂-TCT-NH₂ (1.5 g) was quickly added and the mixture was stirred for 2 h at room temperature. The mixture was then separated by an external magnet, washed with deionized water, sodium carbonate solution (0.1 mol L⁻¹), and acetone and dried at 60 °C to give Fe₃O₄@SiO₂-EDTA NPs. To synthesis the Fe₃O₄@SiO₂-EDTA-Ni NPs, 1.5 g of the as-prepared Fe₃O₄@SiO₂-EDTA nanocomposite and 1 g of nickel(II) acetate tetrahydrate (4 mmol) were dispersed in 10 mL of THF by ultrasonication and stirred for 4 h under reflux conditions. Finally, the products (Fe₃O₄@SiO₂-EDTA-Ni NPs) were collected by a magnet, washed with water and ethanol several times, and dried at 60 °C overnight.

EG Monosodium Salt. According to the approach reported previously,⁷⁰ 300 g of EG (4.83 mol) and 176 g of NaOH (4.39 mol) were first mixed in xylenes (3 L). Then, the mixture was stirred under reflux conditions with a Dean–Stark trap until H₂O separation was finished. Next, the obtained mixture was cooled to room temperature and the precipitate was filtered, washed with xylenes (3 × 100 mL) and *t*-BuOMe (3 × 125 mL), dried in vacuo, and finally, stored under argon.

General Procedure for Suzuki–Miyaura Reactions Using Fe₃O₄@SiO₂-EDTA-Ni(II) NPs. Aryl carbamate and/or aryl sulfamate (1 mmol), arylboronic acid (1 mmol), sodium monoethylene glycolate (0.17 g, 2 equiv), Fe₃O₄@SiO₂-EDTA-Ni(II) NPs (0.018 g, 1 mol % Ni(II)), and EG (3 mL) were added to a 10 mL round-bottom flask. The flask was heated in an oil bath at 100 °C for an appropriate time with stirring under nitrogen atmosphere. The progress of the reaction was monitored by TLC analysis. After the completion of the reaction, the crude was cooled to room temperature and then the catalyst was separated with an external magnet, washed with ethanol, dried under vacuum, and used directly for the subsequent reaction runs. The organic layer was washed with water to get product precipitates and subsequently, the precipitates were separated by filtration and washed with distilled water 3 times. For more purification in some cases, the impure product (checked by TLC) was extra purified by column chromatography (petroleum ether/ethyl acetate = 10:1 (v/v)) to afford the pure product.

■ ASSOCIATED CONTENT

Supporting Information

The Supporting Information is available free of charge at <https://pubs.acs.org/doi/10.1021/acsomega.9b04450>.

Reaction optimization, general experimental methods, chemicals, IR, ^1H NMR, ^{13}C NMR spectra, and elemental analysis for all compounds, C1–C33 (PDF)

■ AUTHOR INFORMATION

Corresponding Author

Iman Dindarloo Inaloo – Chemistry Department, College of Sciences, Shiraz University, Shiraz 71946 84795, Iran;

orcid.org/0000-0003-0087-4210;

Email: iman.dindarlooinaloo@gmail.com

Authors

Sahar Majnooni – Department of Chemistry, University of Isfahan, Isfahan 81746-73441, Iran

Hassan Eslahi – Chemistry Department, College of Sciences, Shiraz University, Shiraz 71946 84795, Iran

Mohsen Esmaeilpour – Chemistry Department, College of Sciences, Shiraz University, Shiraz 71946 84795, Iran

Complete contact information is available at:

<https://pubs.acs.org/doi/10.1021/acsomega.9b04450>

Notes

The authors declare no competing financial interest.

■ ACKNOWLEDGMENTS

The authors gratefully acknowledge the financial support of this work by the research council of Shiraz University.

■ REFERENCES

(1) Kumar, S.; Yadav, I.; Aswal, V. K.; Kohlbrecher, J. Structure and Interaction of Nanoparticle-Protein Complexes. *Langmuir* **2018**, *34*, 5679–5695.

(2) Macnaghten, P.; Kearnes, M. B.; Wynne, B. Nanotechnology, governance, and public deliberation: what role for the social sciences? *Sci. Commun.* **2005**, *27*, 268–291.

(3) Kango, S.; Kalia, S.; Celli, A.; Njuguna, J.; Habibi, Y.; Kumar, R. Surface modification of inorganic nanoparticles for development of organic-inorganic nanocomposites-A review. *Prog. Polym. Sci.* **2013**, *38*, 1232–1261.

(4) Dewan, A.; Sarmah, M.; Thakur, A. J.; Bharali, P.; Bora, U. Greener Biogenic Approach for the Synthesis of Palladium Nanoparticles Using Papaya Peel: An Eco-Friendly Catalyst for C-C Coupling Reaction. *ACS Omega* **2018**, *3*, 5327–5335.

(5) Karimi, B.; Tavakolian, M.; Mansouri, F.; Vali, H. Nanopalladium on Magnetic Ionic Nanoparticle Network (MINN) as an Efficient and Recyclable Catalyst with High Ionic Density and Dispersibility. *ACS Sustainable Chem. Eng.* **2018**, *7*, 3811–3823.

(6) Wu, L.; Mendoza-Garcia, A.; Li, Q.; Sun, S. Organic phase syntheses of magnetic nanoparticles and their applications. *Chem. Rev.* **2016**, *116*, 10473–10512.

(7) Rodriguez-Arco, L.; Rodriguez, I. A.; Carriel, V.; Bonhome-Espinosa, A. B.; Campos, F.; Kuzhir, P.; Duran, J. D. G.; Lopez-Lopez, M. T. Biocompatible magnetic core-shell nanocomposites for engineered magnetic tissues. *Nanoscale* **2016**, *8*, 8138–8150.

(8) Zhao, Y.; Zumin, Q.; Huang, J. Preparation and analysis of Fe_3O_4 magnetic nanoparticles used as targeted-drug carriers. *Chin. J. Chem. Eng.* **2008**, *16*, 451–455.

(9) Sardarian, A. R.; Zangiabadi, M.; Inaloo, I. D. $\text{Fe}_3\text{O}_4/\text{SiO}_2$ /Schiff base/Pd complex as an efficient heterogeneous and recyclable nanocatalyst for chemoselective N-arylation of O-alkyl primary carbamates. *RSC Adv.* **2016**, *6*, 92057–92064.

(10) Deng, Y.; Cai, Y.; Sun, Z.; Liu, J.; Liu, C.; Wei, J.; Li, W.; Liu, C.; Wang, Y.; Zhao, D. Multifunctional mesoporous composite microspheres with well-designed nanostructure: a highly integrated catalyst system. *J. Am. Chem. Soc.* **2010**, *132*, 8466–8473.

(11) Gawande, M. B.; Monga, Y.; Zboril, R.; Sharma, R. K. Silica-decorated magnetic nanocomposites for catalytic applications. *Coord. Chem. Rev.* **2015**, *288*, 118–143.

(12) Liu, R.; Guo, Y.; Odusote, G.; Qu, F.; Priestley, R. D. Core-shell Fe_3O_4 polydopamine nanoparticles serve multipurpose as drug carrier, catalyst support and carbon adsorbent. *ACS Appl. Mater. Interfaces* **2013**, *5*, 9167–9171.

(13) Li, J.-F.; Zhang, Y.-J.; Ding, S.-Y.; Panneerselvam, R.; Tian, Z.-Q. Core-Shell Nanoparticle-Enhanced Raman Spectroscopy. *Chem. Rev.* **2017**, *117*, 5002–5069.

(14) Ghosh Chaudhuri, R.; Paria, S. Core/shell nanoparticles: classes, properties, synthesis mechanisms, characterization, and applications. *Chem. Rev.* **2011**, *112*, 2373–2433.

(15) Polshettiwar, V.; Luque, R.; Fihri, A.; Zhu, H.; Bouhrara, M.; Basset, J.-M. Magnetically recoverable nanocatalysts. *Chem. Rev.* **2011**, *111*, 3036–3075.

(16) Wang, D.; Astruc, D. Fast-growing field of magnetically recyclable nanocatalysts. *Chem. Rev.* **2014**, *114*, 6949–6985.

(17) Miyaura, N.; Suzuki, A. Palladium-catalyzed cross-coupling reactions of organoboron compounds. *Chem. Rev.* **1995**, *95*, 2457–2483.

(18) Rygus, J. P. G.; Crudden, C. M. Enantiospecific and Iterative Suzuki-Miyaura Cross-Couplings. *J. Am. Chem. Soc.* **2017**, *139*, 18124–18137.

(19) Han, F.-S. Transition-metal-catalyzed Suzuki-Miyaura cross-coupling reactions: a remarkable advance from palladium to nickel catalysts. *Chem. Soc. Rev.* **2013**, *42*, 5270–5298.

(20) Balcells, D.; Nova, A. Designing Pd and Ni catalysts for cross-coupling reactions by minimizing off-cycle species. *ACS Catal.* **2018**, *8*, 3499–3515.

(21) Fuentes-Rivera, J. J.; Zick, M. E.; Düfert, M. A.; Milner, P. J. Overcoming Halide Inhibition of Suzuki-Miyaura Couplings with Biaryl Monophosphine-Based Catalysts. *Org. Process Res. Dev.* **2019**, *23*, 1631–1637.

(22) Saptal, V. B.; Saptal, M. V.; Mane, R. S.; Sasaki, T.; Bhanage, B. M. Amine-Functionalized Graphene Oxide-Stabilized Pd Nanoparticles (Pd@APGO): A Novel and Efficient Catalyst for the Suzuki and Carbonylative Suzuki-Miyaura Coupling Reactions. *ACS Omega* **2019**, *4*, 643–649.

(23) Zhou, X.; Guo, X.; Jian, F.; Wei, G. Highly efficient method for Suzuki reactions in aqueous media. *ACS Omega* **2018**, *3*, 4418–4422.

(24) Ohsumi, M.; Nishiwaki, N. Selective Synthesis of (Benzyl)-biphenyls by Successive Suzuki-Miyaura Coupling of Phenylboronic Acids with 4-Bromobenzyl Acetate under Air Atmosphere. *ACS Omega* **2017**, *2*, 7767–7771.

(25) Bayan, R.; Karak, N. Photo-Assisted Synthesis of a Pd-Ag@CQD Nanohybrid and Its Catalytic Efficiency in Promoting the Suzuki-Miyaura Cross-Coupling Reaction under Ligand-Free and Ambient Conditions. *ACS Omega* **2017**, *2*, 8868–8876.

(26) Saito, S.; Oh-tani, S.; Miyaura, N. Synthesis of Biaryls via a Nickel(0)-Catalyzed Cross-Coupling Reaction of Chloroarenes with Arylboronic Acids. *J. Org. Chem.* **1997**, *62*, 8024–8030.

(27) Dehghani, M.; Tadjarodi, A.; Chamani, S. Synthesis and Characterization of Magnetic Zeolite Y-Palladium-Nickel Ferrite by Ultrasonic Irradiation and Investigating Its Catalytic Activity in Suzuki-Miyaura Cross-Coupling Reactions. *ACS Omega* **2019**, *4*, 10640–10648.

(28) Chatupheeraphat, A.; Liao, H.-H.; Srimontree, W.; Guo, L.; Minenkov, Y.; Poater, A.; Cavallo, L.; Rueping, M. Ligand-controlled chemoselective C (acyl)–O bond vs C (aryl)–C bond activation of aromatic esters in nickel catalyzed C (sp_2)–C (sp_3) cross-couplings. *J. Am. Chem. Soc.* **2018**, *140*, 3724–3735.

(29) Schwarzer, M. C.; Konno, R.; Hojo, T.; Ohtsuki, A.; Nakamura, K.; Yasutome, A.; Takahashi, H.; Shimasaki, T.; Tobisu, M.; Chatani, N.; Mori, S. Combined Theoretical and Experimental Studies of

Nickel-Catalyzed Cross-Coupling of Methoxyarenes with Arylboronic Esters via C-O Bond Cleavage. *J. Am. Chem. Soc.* **2017**, *139*, 10347–10358.

(30) Chen, H.; Huang, Z.; Hu, X.; Tang, G.; Xu, P.; Zhao, Y.; Cheng, C.-H. Nickel-catalyzed cross-coupling of aryl phosphates with arylboronic acids. *J. Org. Chem.* **2011**, *76*, 2338–2344.

(31) Harris, M. R.; Hanna, L. E.; Greene, M. A.; Moore, C. E.; Jarvo, E. R. Retention or inversion in stereospecific nickel-catalyzed cross-coupling of benzylic carbamates with arylboronic esters: control of absolute stereochemistry with an achiral catalyst. *J. Am. Chem. Soc.* **2013**, *135*, 3303–3306.

(32) Sardarian, A. R.; Inaloo, I. D. 4-Dodecylbenzenesulfonic acid (DBSA) promoted solvent-free diversity-oriented synthesis of primary carbamates, S-thiocarbamates and ureas. *RSC Adv.* **2015**, *5*, 76626–76641.

(33) Inaloo, I. D.; Majnooni, S. Eco-Efficient Ultrasonic-Responsive Synthesis of Primary O-Alkyl and O-Aryl Thiocarbamates Using Brønsted Acid Ionic Liquid [H-NMP][HSO₄] in Aqueous Media at Room Temperature. *ChemistrySelect* **2018**, *3*, 4095–4100.

(34) Modarresi-Alam, A. R.; Inaloo, I. D.; Kleinpeter, E. Synthesis of primary thiocarbamates by silica sulfuric acid as effective reagent under solid-state and solution conditions. *J. Mol. Struct.* **2012**, *1024*, 156–162.

(35) Antoft-Finch, A.; Blackburn, T.; Snieckus, V. N,N-DiethylO-Carbamate: Directed Metalation Group and Orthogonal Suzuki-Miyaura Cross-Coupling Partner. *J. Am. Chem. Soc.* **2009**, *131*, 17750–17752.

(36) Wang, Y.; Wu, S.-B.; Shi, W.-J.; Shi, Z.-J. C-O/C-H Coupling of Polyfluoroarenes with Aryl Carbamates by Cooperative Ni/Cu Catalysis. *Org. Lett.* **2016**, *18*, 2548–2551.

(37) Rosen, B. M.; Quasdorf, K. W.; Wilson, D. A.; Zhang, N.; Resmerita, A.-M.; Garg, N. K.; Percec, V. Nickel-Catalyzed Cross-Couplings Involving Carbon–Oxygen Bonds. *Chem. Rev.* **2011**, *111*, 1346–1416.

(38) Sardarian, A. R.; Dindarloo Inaloo, I.; Zangiabadi, M. Selective Synthesis of Secondary Arylcarbamates via Efficient and Cost Effective Copper-Catalyzed Mono Arylation of Primary Carbamates with Aryl Halides and Arylboronic Acids. *Catal. Lett.* **2018**, *148*, 642–652.

(39) Inaloo, I. D.; Majnooni, S. Ureas as safe carbonyl sources for the synthesis of carbamates with deep eutectic solvents (DESs) as efficient and recyclable solvent/catalyst systems. *New J. Chem.* **2018**, *42*, 13249–13255.

(40) Sardarian, A. R.; Inaloo, I. D.; Modarresi-Alam, A. R. Highly efficient synthesis of alkyl and aryl primary thiocarbamates and dithiocarbamates under metal- and solvent-free conditions. *Mol. Diversity* **2018**, *22*, 863–878.

(41) Ohtsuki, A.; Yanagisawa, K.; Furukawa, T.; Tobisu, M.; Chatani, N. Nickel/N-Heterocyclic Carbene-Catalyzed Suzuki-Miyaura Type Cross-Coupling of Aryl Carbamates. *J. Org. Chem.* **2016**, *81*, 9409–9414.

(42) Muto, K.; Hatakeyama, T.; Yamaguchi, J.; Itami, K. C-H arylation and alkenylation of imidazoles by nickel catalysis: solvent-accelerated imidazole C-H activation. *Chem. Sci.* **2015**, *6*, 6792–6798.

(43) Ehle, A. R.; Zhou, Q.; Watson, M. P. Nickel(0)-Catalyzed Heck Cross-Coupling via Activation of Aryl C-OPiv Bonds. *Org. Lett.* **2012**, *14*, 1202–1205.

(44) Sardzinski, L. W.; Wertjes, W. C.; Schnaith, A. M.; Kalyani, D. Nickel-Catalyzed Decarboxylative Cross-Coupling of Perfluorobenzoates with Aryl Halides and Sulfonates. *Org. Lett.* **2015**, *17*, 1256–1259.

(45) Wang, M.; Yuan, X.; Li, H.; Ren, L.; Sun, Z.; Hou, Y.; Chu, W. Nickel-catalyzed Suzuki-Miyaura cross-coupling reactions of aryl halides with arylboronic acids in ionic liquids. *Catal. Commun.* **2015**, *58*, 154–157.

(46) Ke, H.; Chen, X.; Zou, G. N-Heterocyclic Carbene-Assisted, Bis(phosphine)nickel-Catalyzed Cross-Couplings of Diarylboronic Acids with Aryl Chlorides, Tosylates, and Sulfamates. *J. Org. Chem.* **2014**, *79*, 7132–7140.

(47) Tobisu, M.; Xu, T.; Shimasaki, T.; Chatani, N. Nickel-Catalyzed Suzuki-Miyaura Reaction of Aryl Fluorides. *J. Am. Chem. Soc.* **2011**, *133*, 19505–19511.

(48) Magano, J.; Monfette, S. Development of an air-stable, broadly applicable nickel source for nickel-catalyzed cross-coupling. *ACS Catal.* **2015**, *5*, 3120–3123.

(49) (a) Park, N. H.; Teverovskiy, G.; Buchwald, S. L. Development of an air-stable nickel precatalyst for the amination of aryl chlorides, sulfamates, mesylates, and triflates. *Org. Lett.* **2014**, *16*, 220–223.

(50) Shields, J. D.; Gray, E. E.; Doyle, A. G. A Modular, Air-Stable Nickel Precatalyst. *Org. Lett.* **2015**, *17*, 2166–2169.

(51) Nattmann, L.; Saeb, R.; Nöthling, N.; Cornella, J. An air-stable binary Ni(0)-olefin catalyst. *Nat. Catal.* **2020**, *3*, 6–13.

(52) Mohadjer Beromi, M.; Nova, A.; Balcells, D.; Brasacchio, A. M.; Brudvig, G. W.; Guard, L. M.; Hazari, N.; Vinyard, D. J. Mechanistic Study of an Improved Ni Precatalyst for Suzuki-Miyaura Reactions of Aryl Sulfamates: Understanding the Role of Ni(I) Species. *J. Am. Chem. Soc.* **2017**, *139*, 922–936.

(53) Sardarian, A. R.; Dindarloo Inaloo, I.; Modarresi-Alam, A. R.; Kleinpeter, E.; Schilde, U. Metal-Free Regioselective Monocyanation of Hydroxy-, Alkoxy-, and Benzyloxyarenes by Potassium Thiocyanate and Silica Sulfuric Acid as a Cyanating Agent. *J. Org. Chem.* **2019**, *84*, 1748–1756.

(54) Inaloo, I. D.; Majnooni, S. A Fe₃O₄@SiO₂/Schiff Base/Pd Complex as an Efficient Heterogeneous and Recyclable Nanocatalyst for One-Pot Domino Synthesis of Carbamates and Unsymmetrical Ureas. *Eur. J. Org. Chem.* **2019**, *2019*, 6359–6368.

(55) Sardarian, A. R.; Dindarloo Inaloo, I. D.; Zangiabadi, M. An Fe₃O₄@SiO₂/Schiff base/Cu (ii) complex as an efficient recyclable magnetic nanocatalyst for selective mono N-arylation of primary O-alkyl thiocarbamates and primary O-alkyl carbamates with aryl halides and arylboronic acids. *New J. Chem.* **2019**, *43*, 8557–8565.

(56) Inaloo, I. D.; Majnooni, S.; Esmailpour, M. Superparamagnetic Fe₃O₄ Nanoparticles in a Deep Eutectic Solvent: An Efficient and Recyclable Catalytic System for the Synthesis of Primary Carbamates and Monosubstituted Ureas. *Eur. J. Org. Chem.* **2018**, *2018*, 3481–3488.

(57) Esmailpour, M.; Javidi, J.; Zahmatkesh, S. One-pot synthesis of 1-and 5-substituted 1H-tetrazoles using 1, 4-dihydroxyanthraquinone–copper (II) supported on superparamagnetic Fe₃O₄@SiO₂ magnetic porous nanospheres as a recyclable catalyst. *Appl. Organomet. Chem.* **2016**, *30*, 897–904.

(58) Esmailpour, M.; Zahmatkesh, S.; Fahimi, N.; Nosratabadi, M. Palladium nanoparticles immobilized on EDTA-modified Fe₃O₄@SiO₂ nanospheres as an efficient and magnetically separable catalyst for Suzuki and Sonogashira cross-coupling reactions. *Appl. Organomet. Chem.* **2018**, *32*, No. e4302.

(59) Quasdorf, K. W.; Antoft-Finch, A.; Liu, P.; Silberstein, A. L.; Komaromi, A.; Blackburn, T.; Ramgren, S. D.; Houk, K. N.; Snieckus, V.; Garg, N. K. Suzuki-Miyaura Cross-Coupling of Aryl Carbamates and Sulfamates: Experimental and Computational Studies. *J. Am. Chem. Soc.* **2011**, *133*, 6352–6363.

(60) Li, Z.; Liu, L. Recent advances in mechanistic studies on Ni catalyzed cross-coupling reactions. *Chin. J. Catal.* **2015**, *36*, 3–14.

(61) Cheung, M. S.; Sheong, F. K.; Marder, T. B.; Lin, Z. Computational Insight into Nickel-Catalyzed Carbon-Carbon versus Carbon-Boron Coupling Reactions of Primary, Secondary, and Tertiary Alkyl Bromides. *Chem.—Eur. J.* **2015**, *21*, 7480–7488.

(62) Nowrouzi, N.; Zarei, M. NiCl₂·E₆H₂O: an efficient catalyst precursor for phosphine-free Heck and Sonogashira cross-coupling reactions. *Tetrahedron* **2015**, *71*, 7847–7852.

(63) Adhikari, S.; Madras, G. Role of Ni in hetero-architected NiO/Ni composites for enhanced catalytic performance. *Phys. Chem. Chem. Phys.* **2017**, *19*, 13895–13908.

(64) Yung, T.-Y.; Huang, L.-Y.; Chan, T.-Y.; Wang, K.-S.; Liu, T.-Y.; Chen, P.-T.; Chao, C.-Y.; Liu, L.-K. Synthesis and characterizations of Ni-NiO nanoparticles on PDDA-modified graphene for oxygen reduction reaction. *Nanoscale Res. Lett.* **2014**, *9*, 444.

(65) Mastalir, M.; Stöger, B.; Pittenauer, E.; Allmaier, G.; Kirchner, K. Air-Stable Triazine-Based Ni(II) PNP Pincer Complexes As Catalysts for the Suzuki-Miyaura Cross-Coupling. *Org. Lett.* **2016**, *18*, 3186–3189.

(66) Quasdorf, K. W.; Riener, M.; Petrova, K. V.; Garg, N. K. Suzuki–Miyaura Coupling of Aryl Carbamates, Carbonates, and Sulfamates. *J. Am. Chem. Soc.* **2009**, *131*, 17748–17749.

(67) Baghbanzadeh, M.; Pilger, C.; Kappe, C. O. Rapid Nickel-Catalyzed Suzuki–Miyaura Cross-Couplings of Aryl Carbamates and Sulfamates Utilizing Microwave Heating. *J. Org. Chem.* **2011**, *76*, 1507–1510.

(68) Chen, G.-J.; Han, F.-S. An efficient Suzuki–Miyaura coupling of aryl sulfamates and boronic acids catalyzed by NiCl₂(dppp). *Eur. J. Org. Chem.* **2012**, *2012*, 3575–3579.

(69) Li, X.-J.; Zhang, J.-L.; Geng, Y.; Jin, Z. Nickel-Catalyzed Suzuki-Miyaura Coupling of Heteroaryl Ethers with Arylboronic Acids. *J. Org. Chem.* **2013**, *78*, 5078–5084.

(70) Grygorenko, O. O.; Bondarenko, A. V.; Tolmachev, A. A.; Vashchenko, B. V. Synthesis of Functionalized 1,4-Dioxanes with an Additional (Hetero) Aliphatic Ring. *Synthesis* **2018**, *50*, 3696–3707.